

Structural and dielectric properties of Zn-doped MgAl₂O₄

Tanveer Hussain¹⁾, *Shahid Atiq²⁾, Saira Riaz³⁾ and Shahzad Naseem⁴⁾

*Centre of Excellence in Solid State Physics, University of the Punjab,
Quaid-e-Azam campus, Lahore-54590, Pakistan*

²⁾satiq.cssp@pu.edu.pk

ABSTRACT

MgAl₂O₄ based spinels exhibit fascinating microwave dielectric characteristics. However, the phase pure synthesis of these compounds usually requires a high processing temperature. Here, we report relatively low temperature synthesis of MgAl₂O₄ ceramics by sol-gel based microwave assisted combustion process. Zn was substituted at Mg site in order to systematically investigate its effect on the structural and dielectric statistics. X-ray diffraction was utilized to confirm the crystal structure and to evaluate the structural parameters. Surface morphology was determined by using a scanning electron microscope. The effects of Zn substitution at Mg-site on frequency dependent dielectric constant and tangent loss have been reported in detail.

1. INTRODUCTION

Spinel cover a very important group of ceramic materials possessing structural properties leading to desirable catalytic, mechanical, optical and electrical properties [Ueda et al., 1992]. Having general formula AB₂O₄, the spinels are basically non-silicate oxides, found in earth's crust [Kushwaha et al., 2013]. Spinel hold a highly packed cubic symmetry which belongs to space group of Fd3m. An important characteristic feature of spinel is their ability to hold large number of divalent and trivalent cations, separated by oxygen positional parameter [Arbi et al., 2012]. Metal cation usually occupies 1/8 of the tetrahedral site and 1/2 of octahedral site with 32 oxygen ions in a complete unit cell of spinel structure [Hill et al., 1979].

Owing to its isotropic crystal structure with no birefringence, magnesium aluminate (MgAl₂O₄) based spinel ceramics exhibit excellent transparency in visible and IR-wavelength regions [Fu et al., 2013]. In particular, transparent MgAl₂O₄ ceramics have been investigated extensively due to their versatile physical properties, excellent thermal, mechanical and optoelectronic properties which sustain even at high temperatures [Hosseini et al., 2008]. In the crystal structure of MgAl₂O₄, as shown in Fig. 1, Mg²⁺ hold 8 of 84 tetrahedral positions while Al³⁺ occupies 16 of 32 octahedral sites. Such features of the crystal structure enable it prospective for the injecting luminescence activators with 2 or 3 valence charges, in the wide range of concentrations [Beketov et al., 2014]. In this context, MgAl₂O₄ has also been assessed

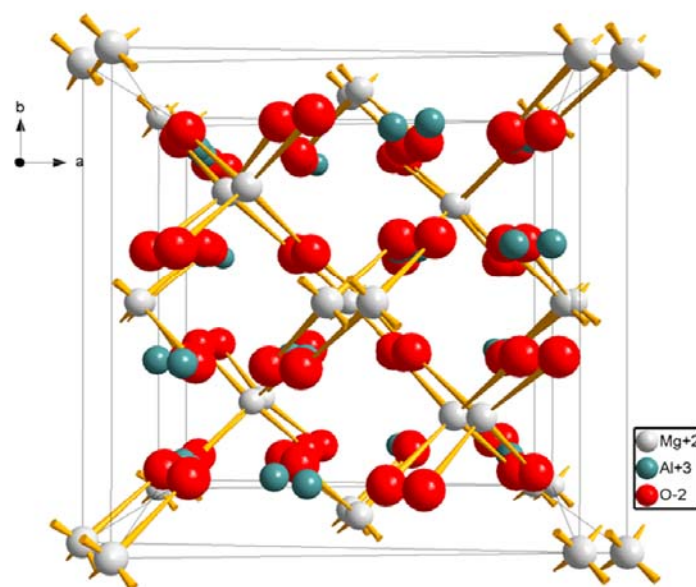


Fig. 1 Crystal structure of $MgAl_2O_4$

as a phosphor host, doped with various ions such as Tb [Omkaram et al., 2008], Eu [Chen et al., 2010], Ti [Sato et al., 2005], Cr [Gluchowski et al., 2009] and Mn [Singh et al., 2007].

On the other hand, $ZnAl_2O_4$ with a band gap of 3.8 – 3.9 eV, and being an electro-conductive material, is considered an excellent choice for ultra-violet (UV) photoelectronic devices [Kumar et al., 2014]. In addition, this material also finds potential applications as catalyst to enhance dehydration, hydrogenation, and dehydrogenation in chemical and petrochemical industries [Lou et al., 2005]. In this context, the substitution of Zn at Mg site in $MgAl_2O_4$ could tailor the band gap of resultant compound in a wide range which would result in such a recipe that could further widen its range of applications. A number of methods for example, solid state reaction [Kashii et al., 1999], precipitation [Alvar et al., 2010], hydrothermal synthesis [Amini et al., 2007], and sol gel [Rezgui et al., 1997] are available for synthesis of these spinel compounds. However, sol-gel based auto-combustion technique [Ianos et al., 2009] has emerged as the most efficient route to synthesize oxide materials in a quick time with less consumption of energy.

2. EXPERIMENTAL PROCEDURE

Single phase samples of pure and Zn-doped $MgAl_2O_4$ having general formula as $Mg_{1-x}Zn_xAl_2O_4$ ($x = 0.0, 0.2, 0.4, 0.6, 0.8$ and 1.0) were prepared by using sol-gel based auto-combustion technique. The analytical grade starting reagents such as magnesium nitrate [$Mg(NO_3)_2 \cdot 6H_2O$], zinc nitrate [$Zn(NO_3)_2 \cdot 6H_2O$], aluminum nitrate [$Al(NO_3)_3 \cdot 9H_2O$] and citric acid [$C_6H_8O_7$] (used as a fuel) were mixed in 100 mL of water in stoichiometric amounts adjusting the metal nitrate (MN) to (CA) ratio of 1:2. The precise amounts of the reagents were weighed using a digital balance. The solution

was stirred using a magnetic stirrer and heated at 90 °C on a hot plate for two hours to get a gel. The whole set up was placed in an ESCO fume hood. When the gel was formed, magnetic stirrer was taken out of the gel and the temperature of the hotplate was raised up to 300°C which led to the complete combustion of the gel within a few moments. The final product was a loose and fluffy powder having brownish grey color. The powder samples were then calcined at 950 °C in a muffle furnace for two hours. After calcination, the color of the powder was changed to white. The samples were palletized having diameter of 10 mm using an Apex hydraulic press by applying a pressure 5.25 ton and then the samples were sintered at 600 °C for two hours to harden the pellets.

A Bruker D/8 X-ray diffractometer (XRD) with $\text{CuK}\alpha$ radiations (1.5418Å) was used to record the diffraction patterns of powder samples to verify the formation of desired phase of the material. Surface morphology of the samples in the pallet form was investigated by a Hitachi S-3400N scanning electron microscope (SEM). Frequency (100Hz-10MHz) dependent dielectric characteristics of the ceramic samples were analyzed by a Wien-Kerr Precision Impedance Analyzer.

3. RESULTS AND DISCUSSION

Fig. 2 shows the XRD patterns of the series of samples having general formula $\text{Mg}_{1-x}\text{Zn}_x\text{Al}_2\text{O}_4$ ($x = 0.0, 0.2, 0.4, 0.6, 0.8$ and 1.0) obtained in the 2θ range of 10 - 80°. The pattern shown in Fig. 2(a) has been matched with ICSD reference code no. 00-021-1152, having cubic spinel structure characteristic of MgAl_2O_4 . The material belongs to space group no. $\text{Fd}\bar{3}\text{m}$, having lattice constant 8.0831 Å, unit cell volume 528.12 Å³

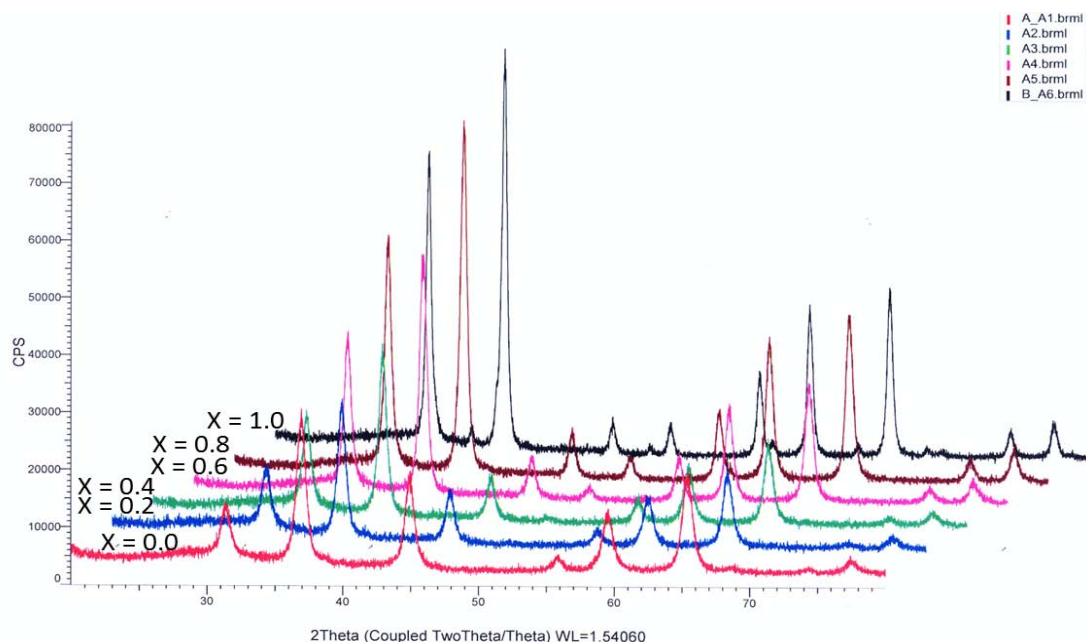


Fig. 2 X-ray diffraction patterns of $\text{Mg}_{1-x}\text{Zn}_x\text{Al}_2\text{O}_4$ ($x = 0.0, 0.2, 0.4, 0.6, 0.8$ and 1.0)

and calculated X-ray density 3.58 g/cm^3 . The pattern shown in Fig. 2(f) has been matched with ICSD reference code no. 00-005-0669, having cubic spinel structure characteristic of ZnAl_2O_4 . The material belongs to space group no. Fd3m, having lattice constant 8.0848 \AA , unit cell volume 528.45 \AA^3 and calculated X-ray density 4.61 g/cm^3 . The patterns have indexed according to the reference codes. It has been observed that all the peaks present in the diffraction patterns belong to the cubic spinel structure, characteristic to the MgAl_2O_4 and ZnAl_2O_4 . No impurity peak or any secondary phase was obvious in the patterns. The patterns shown in Figs. 2(b – e) belong to Zn doped MgAl_2O_4 samples. As the lattice constant of ZnAl_2O_4 is slightly higher than that of MgAl_2O_4 , therefore a slight increase in the lattice constant is expected in the series as one move from $x = 0.0$ to 1.0. This is well justifiable when one observe a small and gradual shift in the peak position.

Fig. 3 shows the structural morphology of the samples, as determined by images obtained using SEM. The figure shows four representative micrographs of the series for $x = 0.0, 0.2, 0.6$ and 1.0 . As the samples are mainly insulating, so no clear grains or grain boundaries were distinguished. However, a few small grains, in the nanometer range, were obvious. Mainly the grains were embedded together to make small and big clusters, consisting of many grains, of micrometer size. Porosity of the samples was not very high as a few very few black spots were visible that suggested that the material would be mechanically very strong.

The electric response of a material can be described by its dielectric parameters, i.e., dielectric constant (ϵ'), dielectric tangent loss ($\text{Tan}\delta$) and dielectric loss factor (ϵ''). In order to investigate the dielectric properties of $\text{Mg}_{1-x}\text{Zn}_x\text{Al}_2\text{O}_4$ ($x = 0.0, 0.2, 0.4, 0.6, 0.8$

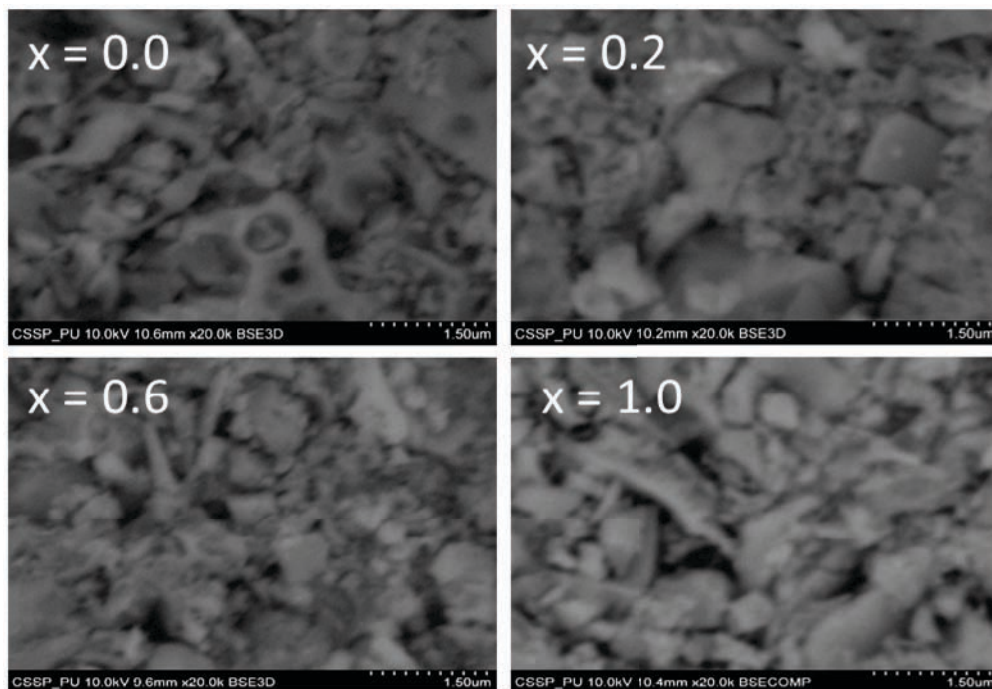


Fig. 3 SEM images of $\text{Mg}_{1-x}\text{Zn}_x\text{Al}_2\text{O}_4$ ($x = 0.0, 0.2, 0.6$ and 1.0)

and 1.0) samples, frequency dependent ϵ' and $\tan\delta$ were determined in the frequency range of 100 Hz to 10 MHz at room temperature (RT). The samples were used in disk form having a diameter of 10 mm and with varying thickness. The values of parallel capacitance and resistance were obtained as a function of frequency for all the samples. The dielectric constant was determined from the relation [Ashiq et al., 2009],

$$\epsilon' = Ct / \epsilon_0 A \quad (1)$$

where 'C' is the capacitance of the pallet in farad, 't' is the thickness of the pallet in meters, 'A' is the cross-sectional area of the flat surface of the pallet and ' ϵ_0 ' is the permittivity of free space. The tangent of dielectric loss angle can be evaluated using the relation given as,

$$\tan\delta = 1/2\pi f C_p R_p \quad (2)$$

where ' δ ' is the loss angle, 'f' is the frequency, ' R_p ' is the equivalent parallel resistance and ' C_p ' is the equivalent parallel capacitance. The dielectric loss factor was also measured in terms of tangent loss factor defined by the relation,

$$\epsilon'' = \epsilon' \tan\delta \quad (3)$$

Fig. 4 shows ϵ' as a function of frequency for all the samples. As can be seen in the figure, ϵ' decreases rapidly with the increase in frequency and becomes independent at high frequencies. The decrease in ϵ' at high frequencies is mainly due to the dielectric relaxation. The dielectric dispersion can be explained by Koop's theory. According to this theory, the dielectric structure is considered to be consisting of double layers, where one layer is conducting and other one is insulating. The dielectric relaxation is directly linked to orientation polarization. On applying external field, atoms of the dielectric material takes some time to align them in the direction of applied electric field, known as relaxation time which is usually of nano second scale.

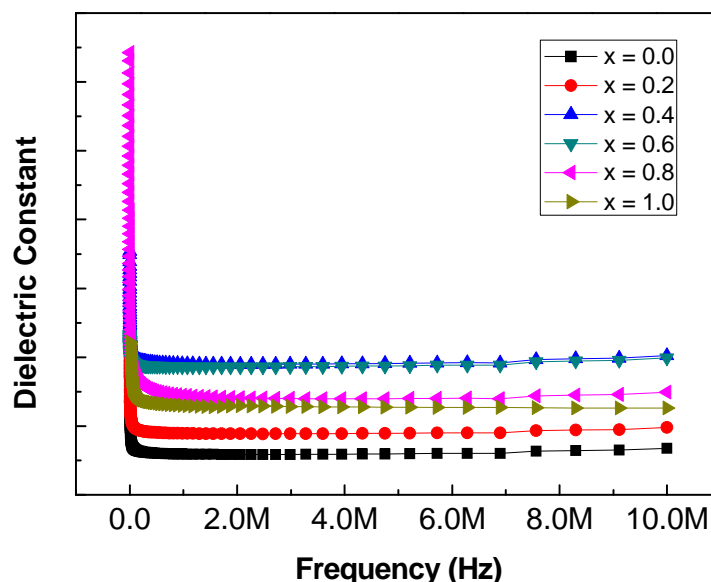


Fig. 4 Frequency dependent dielectric constant of $Mg_{1-x}Zn_xAl_2O_4$ ($x = 0.0, 0.2, 0.4, 0.6, 0.8$ and 1.0)

It is believed that the decrease in ϵ' with increasing frequency is due to the fact that atoms in dielectric material needs a finite time to align up their axis in the applied field direction. As the frequency of the electric field increases, a point is reached when charge carrier of dielectric material do not align with the applied field so polarization cannot reach at its saturation point and do not follow the fluctuations of applied electric field. As a consequence, ϵ' is decreased. When the frequency of the applied field is continuously increased, finally a stage comes when the polarization starts to move before the field reverses and makes no contribution to polarization. Therefore, ϵ' becomes independent at very high frequency. Another valid point for this decrease in dielectric constant is related with the hopping of electrons between the cations residing at octahedral and tetrahedral sites within the ferrite structure, which require a specific amount of energy [Ashiq et al., 2009]. At low frequencies, electric field does not provide enough energy to electrons. As the frequency of the electric field is increased, it provides sufficient energy and a point is reached when hopping of electrons is started between these sites [Din et al., 2014; Verwey et al., 1947], which in turn enhances the conduction mechanism, resulting in reduced dielectric constant. In this case,

$$\omega\tau = 1 \quad (4)$$

where ' τ ' is the relaxation time of the hopping process, ' ω ' is the angular frequency. It is obvious that relaxation time is inversely proportional to the jumping probability per unit time, ' P ', defined as,

$$\tau = P/2 \quad (5)$$

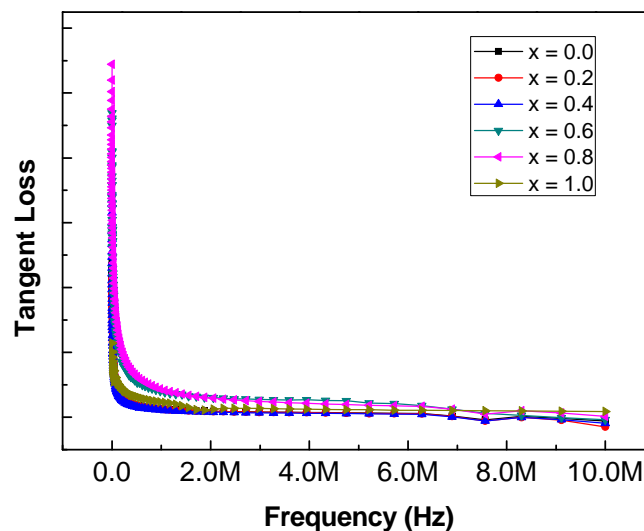


Fig. 5 Frequency dependent tangent loss of $Mg_{1-x}Zn_xAl_2O_4$ ($x = 0.0, 0.2, 0.4, 0.6, 0.8$ and 1.0)

When relaxation time of dielectric material and frequency of the applied field become similar, a phase lag occurs and energy is absorbed in dielectric material, called dielectric loss, directly related with dielectric tangent loss angle. It has been observed that the behavior of tangent loss is similar to ϵ' , as shown in Fig. 5. The dielectric loss of all the samples, $Mg_{1-x}Zn_xAl_2O_4$ ($x = 0.0, 0.2, 0.4, 0.6, 0.8$ and 1.0) is found to decrease with the increase of frequency [Ravinder et al., 2003; Shaikh et al., 1999].

4. CONCLUSIONS

A series of ceramic samples with general formula $Mg_{1-x}Zn_xAl_2O_4$ ($x = 0.0, 0.2, 0.4, 0.6, 0.8$ and 1.0) have been prepared using sol gel auto-ignition route. X-ray diffraction analysis confirmed the cubic spinel structure with space group $Fd3m$. Lattice constant was found to increase slightly from 8.0831 to 8.0848 Å, as Zn was substituted at Mg-site in $MgAl_2O_4$. The images obtained using scanning electron microscope revealed large and small clusters of grains in micrometer range, believed to consist of small grains in nanometer range. The investigation of frequency dependent dielectric parameters revealed conventional ceramic behavior that the values of dielectric parameters were high at low frequency and decreased with the increase in frequency, leading to saturation. The behavior could be related to the conventional dielectric relaxation phenomena.

REFERENCES

- Alvar, E. N., Rezaei, M., and Alvar, H. N. (2010), "Synthesis of mesoporous nanocrystalline $MgAl_2O_4$ spinel via surfactant assisted precipitation route", *Powder Technol.*, **198**(2), 275-278.
- Amini, N. M., Mirzaee, M., and Sepanj, N. (2007), "The effect of solution chemistry on the preparation of $MgAl_2O_4$ by hydrothermal-assisted sol-gel processing", *Mat. Res. Bull.*, **42**(3), 563-570.
- Arbi, M., Benramdane, N., Kebbab, Z., Milaua, R., Chikker, F., and Khenra, R. (2012), "First principles calculations of structural, electronic and optical properties of zinc aluminate oxide", *Mat. Sci. Semicon. Proc.*, **15**(3), 301-307.
- Ashiq, M. N., Iqbal, M. J., Gul, I. H. (2009), "Structural, magnetic and dielectric properties of Zr-Cd substituted strontium hexaferrite ($SrFe_{12}O_{19}$) nanoparticles", *J. Alloy Compd.*, **487**, 341-345.
- Beketov, I. V., Medvedev, A. I., Samatov, O. M., Spirina, A. V., and Shabanova, K. I. (2014), "Synthesis and luminescent properties of $MgAl_2O_4:Eu$ nanopowders", *J. Alloy Compd.*, **586**, S472-S475.
- Chen, X. Y., Ma, C., and Bao, S. P. (2010), " $MgAl_2O_4:Eu^{3+}$ nanoplates and nanoparticles as red-emitting phosphors: Shape-controlled synthesis and photoluminescent properties", *Solid State Sci.*, **12**(5), 857-863.
- Din, M. F., Ahmad, I., Ahmad, M., Farid, M. T., Iqbal, M. A., Murtaza, G., Akhtar, M. N., Shakir, I., Warsi, M. F., and Khan, M. A. (2014), "Influence of Cd substitution on structural, electrical and magnetic properties of M-type barium hexaferrites co-precipitated nanomaterials", *J. Alloy Compd.*, **584**, 646-651.

- Fu, P., Lu, W., Lei, W., Xu, Y., Wang, X., and Wu, J., (2013), "Transparent polycrystalline $MgAl_2O_4$ ceramic fabricated by spark plasma sintering: Microwave dielectric and optical properties", *Ceram. Int.*, **39**(3), 2481-2487.
- Gluchowski, P., Pazik, R., Hreniak, D., Strek, W. (2009), "Luminescence studies of Cr^{3+} doped $MgAl_2O_4$ nanocrystalline powders", *Chem. Phys.*, **358**(1-2), 52-56.
- Hill R. J., Graig, J. R., and Gibbs, G. V. (1979), "Systematics of the spinel structure type", *Phys. Chem. Miner.*, **4**(4), 317-339.
- Hosseini, S. M. (2008), "Structural, electronic and optical properties of spinel $MgAl_2O_4$ oxide", *Phys. Status Solidi B*, **245**(12), 2609-2615.
- Ianos, R., and Lazau, R. (2009), "Combustion synthesis, characterization and sintering behavior of magnesium aluminate ($MgAl_2O_4$) powders", *Mater. Chem. Phys.*, **115**(2-3), 645-648.
- Kashii, N., Maekawa, H., and Hinatsu, Y. (1999), "Dynamics of the cation mixing of $MgAl_2O_4$ and $ZnAl_2O_4$ spinels", *J. Am. Ceram. Soc.*, **82**(7), 1844-1848.
- Kumar, M., Mohapatra, M., Natarajan, V. (2014), "Luminescence characteristics of blue emitting $ZnAl_2O_4$: Ce nanophosphors", *J. Lumin.*, **149**, 118-124.
- Kushwaha, A. K. (2013), "Vibrational, elastic properties and sound velocities of zinc aluminate spinel", *Comp. Mater. Sci.*, **69**, 505-509.
- Lou, Z., and Hao, J. (2005), "Cathodoluminescent characteristics of green-emitting $ZnAl_2O_4$:Mn thin-film phosphors", *Appl. Phys. A*, **80**(1), 151-154.
- Omaram, I., Raju, G. S. R., and Buddhudu, S. (2008), "Emission analysis of Tb^{3+} : $MgAl_2O_4$ powder phosphor", *J. Phys. Chem. Solids*, **69**(8), 2066-2069.
- Ravinder, D., and Reddy P. V. B. (2003), "High-frequency dielectric behaviour of Li-Mg ferrites", *Mater. Lett.*, **57**(26-27), 4344-4350.
- Rezgui, S., and Gates, B. C. (1997), "Control of magnesia-alumina properties by acetic acid in sol-gel synthesis", *J. Non-Cryst. Solids*, **210**(2-3), 287-297.
- Sato, T., Shiraib, M., Tanakab, K., Kawabea, Y., and Hanamur, E. (2005), "Strong blue emission from Ti doped $MgAl_2O_4$ crystals", *J. Lumin.*, **114**(2), 155-161.
- Shaikh, A. M., Belled, S. S., and Chougule, B. K. (1999), "Temperature and frequency-dependent dielectric properties of Zn substituted Li-Mg ferrites", *J. Magn. Magn. Mater.*, **195**(2), 384-390.
- Singh V., Chakradhar, R. P. S., Tao, J. L., and Kim, D. K. (2007), "Synthesis, characterization, photoluminescence and EPR investigations of Mn doped $MgAl_2O_4$ phosphors", *J. Solid State Chem.*, **180**(7), 2067-2074.
- Ueda, N., Omata, T., Hikuma, N., Hashimoto, T., and Kawazoe, H. (1992), "New oxide phase with wide band gap and high electronegativity, $MgIn_2O_4$ ", *Appl. Phys. Lett.*, **61**(16), 1954-1955.
- Verwey, E. J., Haayan, P. W., and Romeijn, F. C. (1947), "Physical Properties and Cation Arrangement of Oxides with Spinel Structures II. Electronic Conductivity", *J. Chem. Phys.*, **15**(4), 181-187.